Characteristics of Fibers Formed by Cytochrome *c* and Induced by Anionic Phospholipids†

Juha-Matti Alakoskela,‡ Arimatti Jutila,‡ Adam C. Simonsen,§ Jussi Pirneskoski,‡ Sinikka Pyhäjoki,|| Raija Turunen,|| Sani Marttila,|| Ole G. Mouritsen,§ Erik Goormaghtigh,⊥ and Paavo K. J. Kinnunen*,‡,§

Helsinki Biophysics and Biomembrane Group, Institute of Biomedicine/Biochemistry, P.O. Box 63, University of Helsinki, 00014 Helsinki, Finland, MEMPHYS, Center for Biomembrane Physics, Physics Department, University of Southern Denmark, Campusvej 55, DK-5230 Odense M, Denmark, Crime Laboratory, National Bureau of Investigations, P.O. Box 285, 01301 Vantaa, Finland, and Free University of Brussels, Campus Plaine CP 206/2, Boulevard du Triomphe, 1050 Brussels, Belgium

Received June 5, 2006; Revised Manuscript Received September 7, 2006

ABSTRACT: Recent publications described the formation of millimeter-length fibers by diverse lipid-binding proteins (e.g., histone H1, cytochrome *c*, indolicidin, and endostatin) when they are mixed with 80:20 phosphatidylcholine/phosphatidylserine vesicles. Further, these fibers displayed amyloid characteristics when stained with Congo Red. In the study presented here, we found by FTIR the amide I absorption band to reveal significant variation in fibers formed by cytochrome *c*, with some consisting of cytochrome *c* in a nativelike conformation and some exhibiting strong amyloid (β-sheet) characteristics. Protein structure also varied from amyloid to nearly native within single fibers. Fibers were frequently blue or bluish and sometimes iridescent, likely due to interference of light in the fibers. The amyloid-type amide I band was observed for blue fibers only. AFM shows that fibers consist of smaller 3−4 nm diameter fibers with 10 nm lateral spacing.

The involvement of amyloids in the pathogenesis of several diseases, such as AA-amyloidosis, Alzheimer's disease (*1*), and type II diabetes (*2*), is well-established. In Alzheimer's disease, which is the most common cause of dementia, the formation of amyloid fibrils is preceded by the formation of prefibrillar aggregates, which has been suggested to be the reason for synaptic failure (*3*) as the membrane becomes permeable to ions (*4*, *5*). The formation of the ion channel requires the presence of anionic lipids (*6*), and the conductivity of these channels varies depending on the size of the aggregate (*4*, *7*). The latter is likely to depend on the membrane concentration of the peptide as shown for antimicrobial peptides forming similar channels (*5*). Interestingly, proteins not known to form amyloid in vivo undergo this characteristic transition in a proper solvent environment, thus suggesting that this process can be triggered even for normally nonamyloidogenic proteins. Accordingly, differences in the amyloidogenicity of proteins are quantitative, not qualitative (*8*).

Possibilities for the modulation of the solvent environment in vivo are rather limited. There is, however, evidence to suggest that electrostatic interactions with negatively charged lipids are important for membrane association, aggregation, and formation of amyloid fibers by amyloid-β peptides (*9*−*14*), yet lipid peroxidation products also enhance the formation of Aβ amyloid (*15*). We recently observed acidic phospholipid-induced formation of very large, 0.1−4.0 mm long lipid−protein fibers by several proteins and peptides, viz., lysozyme, insulin, glyceraldehyde-3-phosphate dehydrogenase, myoglobin, transthyretin, cytochrome *c*, histone H1, α-lactalbumin, endostatin, and antimicrobial peptides temporin L, magainin, and indolicidin (*16*, *17*). Yamamoto et al. (*18*) showed that sodium dodecyl sulfate enhances the amyloid formation by β_2-microglobulin, and similarly, Knight and Miranker (*19*) showed that negatively charged phospholipid vesicles catalyze amyloid fiber formation by the islet amyloidogenic polypeptide, with gross changes in vesicle morphology. Accordingly, lipid membranes could provide for the low-polarity, acidic environment enhancing the formation of amyloids. Obviously, a membrane surface may in addition act as a highly orienting factor, which can be expected to further enhance protein polymerization. Such effects would readily comply with the general catalytic role suggested for negatively charged phospholipid surfaces in amyloid formation in a physiological environment (*16*, *17*, *20*).

When stained with Congo Red, the acidic phospholipid-induced fibers observed by Zhao et al. (*16*, *17*) demonstrated gold and light green birefringence, generally taken as a characteristic of amyloid. However, the specificity of any dye association method in a complex environment such as a lipid/protein mixture is questionable, especially since Congo Red binds to some extent to both native proteins (*21*) and lipids (*22*). Originally, Congo Red was used as a stain for histological samples that typically undergo extensive prepa-

† This study was supported by COST Action D22, the Sigrid Juselius Foundation, and the Finnish Academy, and J.-M.A. was supported by grants from the Research Foundation of the Orion Corp. and Duodecim.

* To whom correspondence should be addressed: Institute of Biomedicine/Biochemistry, P.O. Box 63, University of Helsinki, 00014 Helsinki, Finland. Telephone: +358 9 19125400. Fax: +358 9 19125444. E-mail: Paavo.Kinnunen@helsinki.fi.

‡ University of Helsinki.

§ University of Southern Denmark.

|| National Bureau of Investigations.

⊥ Free University of Brussels.

10.1021/bi0611107 CCC: $33.50
Published on Web 10/18/2006

ration, such as fixing by formaldehyde, alkaline pH, and washing by organic solvents. Nevertheless, false positives due to cytoskeleton and collagen fibers still arose (*21*, *23*). Further, the twisted, helical structure of the lipid−protein fiber could contribute to the birefringence in the absence of amyloid structure. Positive Congo Red staining is therefore not conclusive evidence but merely an indication of the possible presence of amyloid.

We verified the protein structure in lipid-induced fibers using Fourier transfrom infrared (FTIR)[1] spectroscopy. The amide I absorption band (dominated by C═O stretching) of proteins provides a sensitive probe for detecting the changes in the amount of β-sheets in proteins (*24*, *25*), and the utility of FTIR in studies of amyloid formation has been demonstrated (*15*, *25*, *26*). The large dimensions of the fibers (approximately 5−50 μm in width and 0.1−4 mm in length) exclude transmission FTIR measurements in solution, and poor contact of fibers with the crystal surface compromises ATR−FTIR studies without compression. Yet, the large size of fibers allows one to employ FTIR microscopy (FTIRM), enabling measurements of individual fibers and sections of fibers. This approach was complemented by atomic force microscopy (AFM) that yields data for the structural characteristics of the fibers. FTIRM shows that in many of the blue-colored fibers or sections of fibers cytochrome *c* indeed has an amyloid-like structure while also native or nearly native structures are present. For fibers without a bluish tint, the amyloid-related bands in the IR spectra could not be observed. While it was not possible to investigate the very same fibers by AFM, this technique revealed that some of the fibers consist of smaller fibers with fairly regular spacing. Interestingly, the observation of blue fibers and in some cases iridescence suggests that the structure of the fibers includes periodicity on a 100 nm scale.

EXPERIMENTAL PROCEDURES

Materials. Horse heart cyt *c*, Hepes, and EDTA were from Sigma-Aldrich, and lipids were from Avanti Polar Lipids.

LUV Preparation. Appropriate amounts of the lipid stock solutions were mixed, evaporated to dryness under a gentle nitrogen stream, and then maintained under reduced pressure for a minimum of 1.5 h for the removal of any residual solvent. The dry lipid residues were hydrated with buffer [5 mM HEPES and 0.1 mM EDTA (pH 7.4)], whereafter the suspensions were extensively vortexed, incubated for 30 min at 50−60 °C with continuous shaking, sonicated for 2 min with a bath sonicator, and incubated for an additional 30 min at 50−60 °C. This procedure yields multilamellar vesicles for bilayer-forming uncharged phospholipids as well as for charged phospholipids in the presence of sufficient salt. These solutions were subsequently extruded with a LiposoFast pneumatic low-pressure homogenizer (Avestin, Ottawa, ON) 19 times through Millipore (Bedford, MA) polycarbonate filters (pore size of 100 nm) at a temperature well above the main phase transition temperature of the lipid. This produces mostly unilamellar vesicles whose size distribution depends on the extrusion pore size, the extrusion pressure, and the number of passages of the vesicles through the pores (*27*).

Fiber Formation and Collection Protocol. The amount of protein in buffer needed for the desired lipid:protein ratio was slowly added into a magnetically stirred liposome solution (c = 25 μM) and the solution then incubated overnight. The fibers were photographed and collected under a microscope with micromanipulators and positioned on glass slides. The photographs were typically taken with a 10× objective, yet to obtain picture of a whole fiber, often the final picture had to be constructed of several photographs, both due to the length of fibers and due to fiber curvature requiring adjustment of the focus plane. In these cases, Adobe Photoshop was used to connect the images, and judgment of superimposition of overlapping segments was done by eye.

FTIR Microscopy. Fibers on clean glass slides were flattened by rolling with a roller-blade combination. The flattened fiber was detached from the slide by touching it slightly with a tweezer point or needle, and the fragment was raised on a KBr disk. The fiber was pressed slightly against the disk to produce a good contact. Alternatively, the fiber was placed on the bottom half of a diamond anvil cell and pressed down gently with the top half of the cell. The halves were separated, and the half with the attached fiber was placed on the stage. The interferograms were then collected with a Perkin-Elmer Spectrum 2000 FTIR microscope system and converted to spectra by the use of a strong apodization function. One hundred spectra were averaged to obtain a final spectrum. Handling of the spectral data was performed with a Kinetics software module written by E. Goormaghtigh and with Origin version 5.0 from Microcal Inc. The water vapor spectrum was substracted, whereafter spectra were smoothed to a nominal resolution of 4 cm^{-1}.

Atomic Force Microscopy. Atomic force microscopy was performed using an MFP-3D device (Asylum Research, Santa Barbara, CA) placed on top of a Nikon TE2000 inverted microscope. The fibers were adsorbed to microscope cover glass, and using standard bright field observation and an xy sample stage, the protein fibers were positioned under the AFM cantilever. AFM imaging was done under ambient conditions in tapping mode using NanoSensors cantilevers (NCL-50) with a tapping frequency of ~150 kHz. Note that only the central region of the fibers could be reliably imaged due to the fiber height and the steep slope of the fiber sides.

RESULTS

Although fibers of cyt *c* and lipids invariably formed in the procedure that was used (see Experimental Procedures), their number and appearance were found to vary from sample to sample and even within a single preparation. The length typically varied between 0.1 and 4.0 mm. When the fibers were viewed under a bright field light microscope, clear structural and color differences could be seen in fibers collected from a single incubation. Some relatively straight fibers had ribbonlike segments twisted into a helix (Figure 1B). Some fibers contained more planar ribbons (e.g., Figure 1D), and some had a tendency to fray or had smaller fibers

[1] Abbreviations: AFM, atomic force microscopy; ATR, attenuated total reflection; cyt *c*, cytochrome *c*; d_f, thickness of a film; EDTA, ethylenediaminetetraacetic acid; FTIR(M), Fourier transform infrared (microscopy); HEPES, 4-(2-hydroxyethyl)-1-piperazineethanesulfonic acid; hIAPP, human islet amyloidogenic polypeptide; L:P, lipid:protein; LUV, large unilamellar vesicle; n_f, refractive index of a film; PC, phosphatidylcholine; PG, phosphatidylglycerol; PS, phosphatidylserine; λ, wavelength.

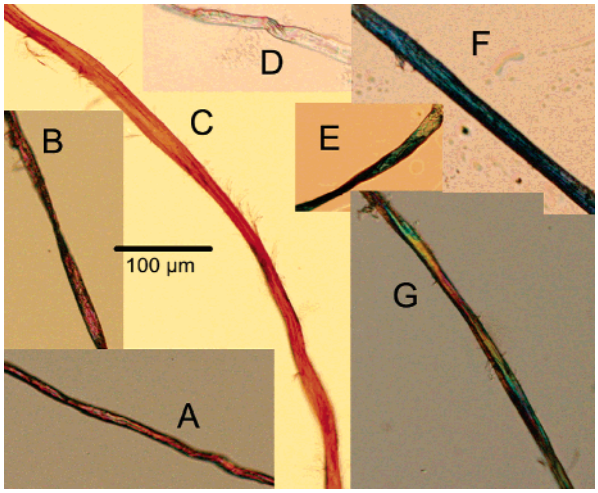

FIGURE 1: Microscopy images for sections of some cyt *c* fibers induced by liposomes. The nominal sample lipid:protein ratios for fibers A−G are 5:1, 100:1, 10:1, 25:1, 10:1, 10:1, and 10:1, respectively. In fibers A, B, D, F, and G, liposomes were composed of PC and PS (80:20), and in fibers C and E, liposomes were composed of PC and PG (80:20). The scale bar applies for all panels.

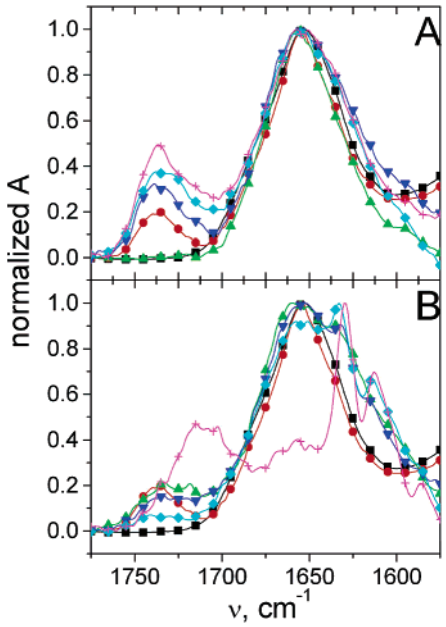

FIGURE 2: (A) FTIR spectra for fibers without bluish tint or amyloid-like peaks. Green triangles, blue triangles, cyan diamonds, and magenta pluses indicate nominal lipid:protein ratios of 5, 25, 50, and 6, respectively. Fiber formation was induced by 80:20 PC/PS liposomes. (B) Spectral bands indicating amyloid structure. Green triangles, blue triangles, cyan diamonds, and magenta pluses indicate nominal lipid:protein ratios of 100, 5, 10, and 10, respectively. The last of these fibers was induced with 80:20 PC/PG liposomes, and the others were induced with 80:20 PC/PS liposomes. In both panels, black squares show the spectra for cyt *c* dried from water onto an ATR crystal and red circles those for cyt *c* and 80:20 PC/PS liposomes with a lipid:protein ratio of 10 dried on an ATR crystal. FTIR spectra of fibers are normalized by peak maximum.

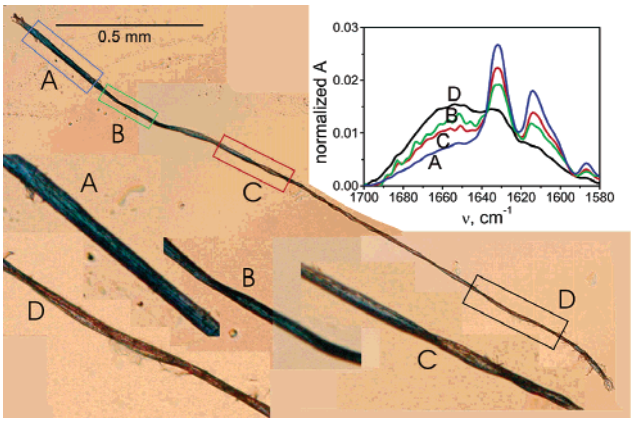

FIGURE 3: Variation of secondary structure along a fiber. Nominal lipid:protein ratio of 10. The positions indicated for the recorded spectra are approximate, as the image was acquired under an optical microscope and spectra were acquired via FTIRM.

sticking out of them (Figure 1C). Consistent with the absorption spectra of native cyt *c*, most fibers were red (Figure 1A−C). However, nearly colorless fibers were also observed (Figure 1D), and some displayed dark blue color or bluish tint (Figure 1E,F). In some fibers, a clear spectrum of colors along the fiber length could be seen (Figure 1G). While the red color obviously derives from the heme group of cyt *c*, the other colors do require alternative explanations, especially since blue color could also be found in fibers formed by other proteins and peptides (e.g., melittin, gelsolin, sakacin P, and temporin B; data not shown). For the sake of clarity, we here report data for cyt *c* only.

Using FTIR microscopy of the cyt *c* fibers, the red and nearly colorless fibers displayed a nativelike spectrum (Figure 2A). For these fibers, the ratio of lipid carbonyl to protein amide I band absorbances showed considerable variation, even when recorded from fibers collected from a single preparation. Some of these bluish fibers displayed a spectrum with clear, sharp, prominent bands at 1631 and 1613 cm^{-1} (Figures 2B and 3, inset), which typically can be attributed to amyloid β-sheet structures (*25*, *26*). For these bluish fibers, the lipid:protein ratio was often low, only a few lipids per cyt *c*. The estimation of the lipid:protein stoichiometry from the measured carbonyl:amide I ratio and comparison with nonfibrous samples with known lipid:protein ratios dried on ATR crystals give, e.g., a lipid:protein ratio of only 2.8 for the PC/PS fiber (cyan diamonds in Figure 2) and 1.0 for the fiber in Figure 3, while one blue fiber induced by 80:20 PC/PG vesicles (magenta pluses in Figure 2) showed very prominent lipid carbonyl bands, suggesting a lipid:protein ratio of approximately 60. The bands characteristic of β-sheets and amyloid could also be observed for some of the bluish fibers formed by proteins other than cyt *c*, implicating that our observations are more generic in nature, in accordance with the reported formation of similar fibers by a large number of different peptides and proteins (*16*, *17*). Remarkably, variation in color and protein structure along single fibers was observed (Figure 3), yet even in a single fiber there appears to be some correlation between fiber color and protein structure, as only weak amyloid spectral features were observed at the red end of the fiber, suggesting that the protein secondary structure and the intermediate scale fiber structure are intimately connected.

The diversity in the structure on the level of whole fibers and protein secondary structure is accompanied by a variation of the surface characteristics of fibers on a more mesoscopic level revealed by AFM. Both smooth surfaces and fiber bundles were seen (Figure 4A). In the former type of samples at large nominal sample lipid:protein ratios, there appear to be structures like distorted or collapsed vesicles on the fiber

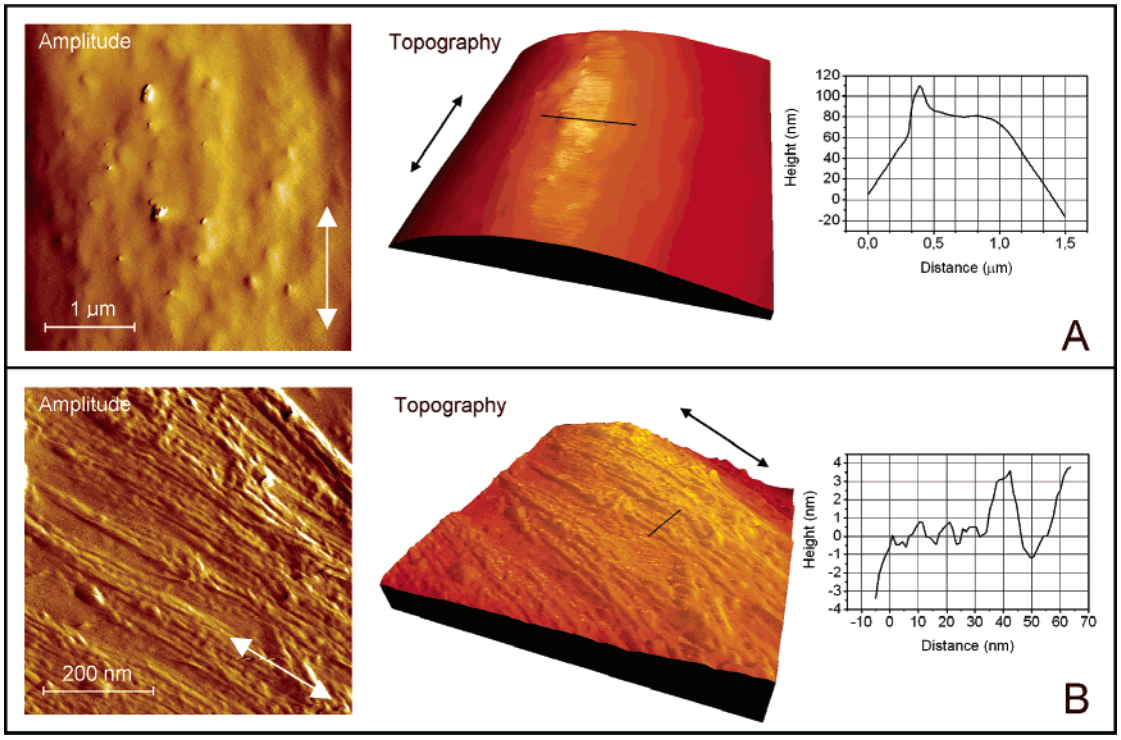

FIGURE 4: AFM images of cytochrome *c* protein fibers. The arrows indicate the orientation of the main fiber long axis. The length scale is indicated by the bar and the height scale by the line scans. A smooth region of a protein fiber (A) shows only a few protruded regions on a smooth surface. A more corrugated fiber region (B) shows that the main fiber is composed of parallel and closely spaced protofibers with an average spacing of 10 nm. Black bars in topography panels indicate the regions corresponding to height vs distance plots shown at the right of the topography panels.

surface. In samples revealing fiber bundles, the protofibers on the fiber surface are 3−4 nm wide, have a fairly regular lateral spacing of approximately 10 nm (Figure 4B), and are oriented parallel to the direction of the long axis of the main fiber. An estimate of a lower limit of 100 nm for the length of this protofiber is provided by the observable length of a protofiber on the fiber surface. Of course, this may not represent the true length of a protofiber, as it may tangle beneath other protofibers and thus be visible for only AFM while residing on the fiber surface.

DISCUSSION

The bluish and in some cases full spectrum of colors exhibited by the fibers in the absence of chromophores is perplexing and is most likely caused by interference (or coherent scattering) of light within these structures. In the simplest scenario of normal incidence and thin film interference due to the upper and lower surfaces of the 3−5 μm thick fiber, we would have maxima in the transmittance coinciding with maxima of $\cos(4\pi n_f d_f/\lambda)$, where n_f, d_f, and λ are the refractive index and thickness of the film and the wavelength in a vacuum, respectively (*28*). If n_f is independent of the wavelength and in the range of $\approx$1.4−1.6 observed for fibrous or crystalline proteins (*29*, *30*), then for fibers that have a thickness of several wavelengths there can be no significant enrichment of blue light as the cosine function will have a large number of maxima in the region of the visible spectrum. A similar problem arises if one considers only protofibers and interprotofiber distances, both of which are much smaller than the wavelength of visible light. Interference related to horizontal layers would require approximately $^1/_4$ wavelength spacing, and we would expect a high level of iridescence, i.e., change in color depending on the angle of observation. While iridescence was indeed observed for some fibers (Figure 1), most of the blue fibers lacked it. Absorption is unlikely to play a significant role, as the same type of coloring could be seen for a number of proteins and peptides (data not shown) as well as for cyt *c* whose heme group is a strong absorber of light. The disappearance of the red color of cyt *c* is intriguing as it suggests that either the covalently attached heme group is lost as a result of conformational changes in cyt *c* or, alternatively, this heme moiety contributes only to the darkness of fibers (see below). Interestingly, quasi-ordered structures formed by collagen fibers of different sizes and interfiber spacings are responsible for both the transparency of cornea and opacity of sclera (*31*, *32*) as well as the various colors of the whole spectrum of colorful skins (and in some cases also feathers) of mammals and birds (*29*, *30*). In these quasi-ordered systems, the distances between neighboring fibers are nearly equal but there is little long-range correlation. This arrangement results in color and either weak iridescence or a lack of it if the fiber size is on the order of $^1/_4$ of the wavelength of light. Thus, a possible candidate for the blue color is a midscale structural arrangement of protofibers, suggesting that in addition to the whole fiber and protofibers with their fairly regular 10 nm lateral distance there is also an intermediate arrangement of fibers into bundles or layers of a width and spacing of approximately 100 nm. While even the smallest fibers seen under a light microscope on surfaces of large fibers (see Figure 1C) are for the reasons of optical resolution necessarily larger than this, obviously they, too, suggest many scales of ordering. Coherent scattering could also explain the loss of the red

color of cyt *c*. Normally, the heme group in cyt *c* absorbs at shorter wavelengths and scatters red light, the protein thus appearing red. This color is lost in blue fibers. As discussed, the heme group may be lost, or alternatively, due to coherent scattering, the fiber scatters only blue light, appearing as blue, and the absorption of heme at blue wavelengths only makes the fiber appear darker.

A striking feature is the variability of the fiber structure, even within a single fiber. In light of the highly variable characteristics described above, it is obvious that we lack control of some additional factors determining the formation of a particular type of structure, yet some kind of fibers (almost) invariably form if the lipid:protein ratio is within certain limits and the lipid concentration is sufficiently low (<100 μM). Slight variation in the temperature or thermal history of liposomes appears to be an unlikely candidate, and the incubation time also does not appear to be crucial. At present, our best guess is that the initial local concentration of the protein is a factor over which we have no control. The variations in fibers may also be derived from the randomness of rare nucleation events, followed by a rapid growth, and thus yielding different kinds of fiber organization depending on the initial nucleus. Unfortunately, the mechanisms of fiber formation remain difficult to assess. Although we have not followed changes in FTIR spectra as a function of time, the conformational heterogeneity within single fibers is unlikely to reflect an ongoing conformational transition, since the appearance of fibers (color and shape) remains more or less unchanged for periods of days. Accordingly, once trapped in a large fiber, the conformational changes appear to become exceedingly slow, proteins retained in more or less frozen, partly metastable conformational states. Once the initial lipid−protein aggregates are formed, the protein fibers within the aggregates are likely to grow predominantly from their ends. Further, subsequent to the formation of amyloid-like conformations, the proteins added to the ends of this protofibril would preferentially adopt this conformation, representing a large decrease in free energy. The interactions between parallel, adjacent protofibrils can be anticipated to be cooperative, thus stabilizing protein conformation in a segment of a fiber. Upon the nucleation of an amyloid-like conformation in a protofibril, these interactions at the growing end of the protofibril bundle will occasionally trigger the transition into an amyloid-like conformation also in the proteins to be added to the protofibrils adjacent to amyloid-like protofibrils. Such triggering of the amyloid-like conformation in adjacent protofibrils during the growth will increase the fraction of the amyloid-like conformation in the direction of growth along the main axis of the main fiber, the more recently grown end having a larger fraction of the amyloid-like conformation. The conformations of the proteins already incorporated in a large fiber are stabilized by the interactions within this fiber. Therefore, the fraction of the amyloid-like conformation could only increase when the fiber is growing, and the proteins newly joined into the fiber would be trapped into either native-like or amyloid-like secondary structure, this secondary structure becoming stabilized upon growth of the main fiber. This model would require interactions between parallel fibers, yet the diameters of and the distance between the protofibers appear to be more or less regular; there probably is periodicity also on the intermediate scale, in keeping with strong cooperative interactions between parallel adjacent fibrils. This conformational heterogeneity may be accompanied by heterogeneity in protein hydration as well.

Considering the role of anionic phospholipids as inducers of fiber formation, it appears likely that electrostatics plays a significant role, especially since fiber formation can be induced for proteins having a positive net charge or clusters of positively charged residues (*16*). The role of anionic lipids in the reorganization may derive from structural destabilization of proteins. First, the environment is more hydrophobic (decreasing the free energy penalty for bringing hydrophobic side chains onto the surface or having hydrophobic clefts). Second, negatively charged phospholipids will compete for interactions with cationic amino acid residues and will tend to destabilize the native protein structure if it either contains salt bridges accessible to lipid or does not allow for optimal interactions between cationic residues and anionic lipids. Indeed, some of the proteins reported to form fibers by Zhao et al. (*16*, *17*) have also been described to adopt the structurally loose molten globule-like state upon association with anionic phospholipids (*33*, *34*). In some cases, local crowding together with the molten globule state could create an amyloid nucleus, which then triggers a transition of the bulk of the aggregated protein into a free energy well represented by the amyloid structure. Detailed studies of the impact of different lipid compositions on amyloid nucleation are warranted and are currently in progress in our laboratory. The content of anionic phospholipid may affect the likelihood of the nucleation of amyloid conformation, yet it is unlikely that a heterogeneous lipid composition of the vesicles as such would explain the conformational heterogeneity of the protein fibrils, as the most pronounced heterogeneity appears on the length scale of thousands of vesicle diameters. Nevertheless, taking into account the apparently crucial role of lipids in triggering amyloid formation and the number of disorders due to amyloid formation, we conclude that the lipid−protein interactions involved in this process present a highly attractive target for drug development.

A model for fiber formation should be able to account for not only the structural factors (3−4 nm protofibers, 10 nm separation, postulated structure on the 100 nm scale, the final size of fibers) but also the variability in protein structure and L:P ratio. The protofiber thickness (Figure 4B) matches the diameter of cyt *c* (*35*) as well as the thickness of the amyloid β-fold (*36*, *37*), while a 100 nm scale could relate to the average diameter of the liposomes that were used. However, the length scale correspondence may be coincidental and derive from nonrelated principles of protofiber organization to higher-level bundles. Nevertheless, as fibers exhibiting interference were detected also with short peptides (for instance, sakacin P and temporin B; data not shown), the 100 nm ordering should derive from very basic interactions between amyloid β-sheets (providing that it is not determined by the vesicle size). In giant vesicle experiments, Menger et al. (*38*) reported that poly-L-lysine permeates bilayers of anionic lipids and that fibers of poly-L-lysine and anionic lipids form inside the giant vesicles, supposedly limited by the vesicle size. This appears to be the case also for histone H1 (*39*). Since cyt *c* in the molten globule state (*40*) as well as peripheral membrane proteins more generally (*41*) have been suggested to penetrate through lipid bilayers, the possibility of cyt *c* fiber formation inside vesicles cannot

be excluded. On the contrary, giant vesicle experiments of Sparr et al. (*42*) with hIAPP suggest that the vesicle outer surface acts as a template structure for the formation of fibers consisting of hIAPP and anionic lipids, followed by the release of phospholipid-containing fibers. Association of cyt *c* with anionic vesicles causes complex changes in solution turbidity and viscosity (*43*, *44*) as well as vesicle morphology (*45*). As cyt *c* is known to induce vesicle aggregation and fusion (*46*), such aggregates could also play a role in fiber formation.

Most importantly, the peaks detected in the IR spectra suggest, especially when evaluated together with the Congo Red staining experiments of our previous studies (*16*, *17*), that proteins in some of the large fibers have adopted an amyloid structure. Accordingly, this study lends support to the suggestion that the exposure of PS on the outer leaflet in various disease states, including cancers and diabetes (*47*), may contribute to the amyloid formation associated with these disorders (*16*, *17*). Our findings demonstrate that it is possible to obain several distinct types of supramolecular lipid−protein structures. It is tempting to speculate that nature would utilize these mechanisms to control cellular functions. This lipid-induced fiber formation has also been suggested to be related to the action of endogenous protein endostatin, which is cytotoxic to cancer cells, as well as to the action of antimicrobial peptides and apoptosis-inducing proteins (*16*, *17*). Nevertheless, while we show that amyloid is present in these fibers formed in vitro, the conditions and concentrations in vivo are very different, and the role of phospholipids in amyloid formation in vivo remains to be established.

REFERENCES

1. Merlini, G., and Westermark, P. (2004) The systemic amyloidoses: Clearer understanding of the molecular mechanisms offers hope for more effective therapies, *J. Intern. Med. 255*, 159−178.
2. Clark, A., and Nilsson, M. R. (2004) Islet amyloid: A complication of islet dysfunction or an etiological factor in type 2 diabetes? *Diabetologia 47*, 157−169.
3. Selkoe, D. J. (2002) Alzheimer's disease is a synaptic failure, *Science 298*, 789−791.
4. Doudevski, I., Lin, H., Azimova, R., Ng, D., Frangione, B., Kagan, B., Ghiso, J., and Lal, R. (2005) Amyloid ion channels: A common structural link for protein-misfolding disease, *Proc. Natl. Acad. Sci. U.S.A. 102*, 10427−10432.
5. Kourie, J. I., and Shorthouse, A. A. (2000) Properties of cytotoxic peptide-formed ion channels, *Am. J. Physiol. 278*, C1063−C1087.
6. Hirakura, Y., Lin, M.-C., and Kagan, B. L. (1999) Alzheimer amyloid Aβ1-42 channels: Effects of solvent, pH, and congo red, *J. Neurosci. Res. 57*, 458−466.
7. Lin, H., Bhatia, R., and Lal, R. (2001) Amyloid 13 protein forms ion channels: Implications for Alzheimer's disease pathophysiology, *FASEB J. 15*, 2433−2444.
8. Fandrich, M., Fletcher, M. A., and Dobson, C. M. (2001) Amyloid fibrils from muscle myoglobin, *Nature 410*, 165−166.
9. Ege, C., and Lee, K. Y. C. (2004) Insertion of Alzheimer's Aβ40 peptide into lipid monolayers, *Biophys. J. 87*, 1732−1740.
10. Kurganov, B., Doh, M., and Arispe, N. (2004) Aggregation of liposomes induced by the toxic peptides Alzheimer's Aβs, human amylin and prion (106−126): Facilitation by membrane-bound GM1 ganglioside, *Peptides 25*, 217−232.
11. Lehtonen, J. Y. A., Holopainen, J. M., and Kinnunen, P. K. J. (1996) Activation of phospholipase A_2 by amyloid β-peptides in vitro, *Biochemistry 35*, 9407−9414.
12. Lindström, F., Bokvist, M., Sparrman, T., and Gröbner, G. (2002) Association of amyloid-β peptide with membrane surfaces monitored by solid state NMR, *Phys. Chem. Chem. Phys. 4*, 5524−5530.
13. Terzi, E., Hölzemann, G., and Seelig, J. (1997) Interaction of Alzheimer β-amyloid peptide(1−40) with lipid membranes, *Biochemistry 36*, 14845−14852.
14. Vargas, J., Alarcon, J. M., and Rojas, E. (2000) Displacement currents associated with the insertion of Alzheimer disease amyloid β-peptide into planar bilayer membranes, *Biophys. J. 79*, 934−944.
15. Koppaka, V., Paul, C., Murray, I. V. J., and Axelsen, P. H. (2003) Early synergy between Aβ42 and oxidatively damaged membranes in promoting amyloid fibril formation by Aβ40, *J. Biol. Chem. 278*, 36277−36284.
16. Zhao, H., Tuominen, E. K. J., and Kinnunen, P. K. J. (2004) Formation of amyloid fibers triggered by phosphatidylserine-containing membranes, *Biochemistry 43*, 10302−10307.
17. Zhao, H., Jutila, A., Nurminen, T., Wickström, S. A., Keski-Oja, J., and Kinnunen, P. K. J. (2005) Binding of endostatin to phosphatidylserine-containing membranes and formation of amyloid-like fibers, *Biochemistry 44*, 2857−2863.
18. Yamamoto, S., Hasegawa, K., Yamaguchi, I., Tsutsumi, S., Kardos, J., Goto, Y., Gejyo, F., and Naiki, H. (2004) Low concentrations of sodium dodecyl sulfate induce the extension of β_2-microglobulin-related amyloid fibrils at a neutral pH, *Biochemistry 43*, 11075−11082.
19. Knight, J. D., and Miranker, A. D. (2004) Phospholipid catalysis of diabetic amyloid assembly, *J. Mol. Biol. 341*, 1175−1187.
20. Gorbenko, G. P., and Kinnunen, P. K. J. (2006) The role of lipid-protein interactions in amyloid-type protein fibril formation, *Chem. Phys. Lipids 141*, 72−82.
21. Khurana, R., Uversky, V. N., Nielsen, L., and Fink, A. L. (2001) Is Congo Red an amyloid-specific dye, *J. Biol. Chem. 276*, 22715−22721.
22. Hahn, C., Kaiser, S., and Wokaun, A. (1996) Interaction of a Congo red dye probe with lecithin vesicles probed by forced Rayleigh scattering, *Tenside, Surfactants, Deterg. 33*, 209−213.
23. Westermark, G. T., Johnson, K. H., and Westermark, P. (1999) Staining methods for identification of amyloid in tissue, *Methods Enzymol. 309*, 3−25.
24. Goormaghtigh, E., Cabiaux, V., and Ruysschaert, J. M. (1990) Secondary structure and dosage of soluble and membrane proteins by attenuated total reflection Fourier-transform infrared spectroscopy on hydrated films, *Eur. J. Biochem. 193*, 409−420.
25. Calero, M., and Gasset, M. (2005) Fourier transform infrared and circular dichroism spectroscopies for amyloid studies, *Methods Mol. Biol. 299*, 129−151.
26. Zandomeneghi, G., Krebs, M. R. H., McCammon, M. G., and Faendrich, M. (2004) FTIR reveals structural differences between native β-sheet proteins and amyloid fibrils, *Protein Sci. 13*, 3314−3321.
27. Berger, N., Sachse, A., Bender, J., Schubert, R., and Brandl, M. (2001) Filter extrusion of liposomes using different devices: Comparison of liposome size, encapsulation efficiency, and process characteristics, *Int. J. Pharm. 223*, 55−68.
28. Heavens, O. S. (1991) *Optical Properties of Thin Solid Films.* Dover, Mineola, NY (republication of work first published in 1955 by Butterworths, London).
29. Prum, R. O., Morrison, R. L., and Ten Eyck, G. R. (1994) Structural color production by constructive reflection from ordered collagen arrays in a bird (*Philepitta castanea*: Eurylaimidae), *J. Morphol. 222*, 61−72.
30. Prum, R. O., and Torres, R. H. (2004) Structural colouration of mammalian skin: Convergent evolution of coherently scattering dermal collagen arrays, *J. Exp. Biol. 207*, 2157−2172.
31. Benedek, G. B. (1971) Theory of transparency of the eye, *Appl. Optics 3*, 459−473.
32. Vaezy, S., and Clark, J. I. (1991) A quantitative analysis of transparency in the human sclera and cornea using Fourier methods, *J. Microsc. 163*, 85−94.
33. Muga, A., Mantsch, H. H., and Surewicz, W. K. (1991) Membrane binding induces destabilization of cytochrome c structure, *Biochemistry 30*, 7219−7224.
34. Bañuelos, S., and Muga, A. (1995) Binding of molten globule-like conformations to lipid bilayers. Structure of native and partially folded α-lactalbumin bound to model membranes, *J. Biol. Chem. 270*, 29910−29915.
35. Dickerson, R. E., Takano, T., Eisenberg, D., Kallai, O. B., Samson, L., Cooper, A., and Margoliash, E. (1971) Ferricytochrome c. I.

General features of the horse and bonito proteins at 2.8 Å resolution, *J. Biol. Chem. 246*, 1511−1535.
36. Tycko, R. (2004) Progress towards a molecular-level structural understanding of amyloid fibrils, *Curr. Opin. Struct. Biol. 14*, 96−103.
37. Lazar, K. L., Miller-Auer, H., Getz, S. G., Orgel, J. P. R. O., and Meredith, S. C. (2005) Helix-turn-helix peptides that form R-helical fibrils: Turn sequences drive fibril structure, *Biochemistry 44*, 12681−12689.
38. Menger, F. M., Seredyuk, V. A., Kitaeva, M. V., Yaroslavov, A. A., and Melik-Nubarov, N. S. (2003) Migration of poly-L-lysine through a lipid bilayer, *J. Am. Chem. Soc. 125*, 2846−2847.
39. Zhao, H., Bose, S., Tuominen, E. K. J., and Kinnunen, P. K. J. (2004) Interactions of histone H1 with phospholipids and comparison of its binding to giant liposomes and human leukemic T cells, *Biochemistry 43*, 10192−10202.
40. Heimburg, T., and Marsh, D. (1995) Protein surface-distribution and protein-protein interactions in the binding of peripheral proteins to charged lipid membranes, *Biophys. J. 68*, 536−546.
41. Zuckermann, M. J., and Heimburg, T. (2001) Insertion and pore formation driven by adsorption of proteins onto lipid bilayer membrane-water interfaces, *Biophys. J. 81*, 2458−2472.
42. Sparr, E., Engel, M. F. M., Sakharov, D. V., Sprong, M., Jacobs, J., de Kruijff, B., Hoppener, J. W. M., and Killian, J. A. (2004) Islet amyloid polypeptide-induced membrane leakage involves uptake of lipids by forming amyloid fibers, *FEBS Lett. 577*, 117−120.
43. Tuominen, E. K., Wallace, C. J., and Kinnunen, P. K. (1997) The invariant ARG91 is required for the rupture of liposomes by cytochrome c, *Biochem. Biophys. Res. Commun. 238*, 140−142.
44. Oellerich, S., Lecomte, S., Paternostre, M., Heimburg, T., and Hildebrandt, P. (2004) Peripheral and integral binding of cytochrome c to phospholipids vesicles, *J. Phys. Chem. B 108*, 3871−3878.
45. Heimburg, T., and Biltonen, R. L. (1994) Thermotropic behavior of dimyristoylphosphatidylglycerol and its interaction with cytochrome c, *Biochemistry 33*, 9477−9488.
46. Lee, S., and Kim, H. (1989) Fusion of phospholipid vesicles mediated by cytochrome c, *Arch. Biochem. Biophys. 271*, 188−199.
47. Balasubramanian, K., and Schroit, A. J. (2003) Aminophospholipid asymmetry: A matter of life and death, *Annu. Rev. Physiol. 65*, 701−734.

BI0611107